A Light-Field Metasurface for High-Resolution Single-Particle Tracking

Aaron L. Holsteen,[†,§] Dianmin Lin,[†,‡,§] Isaac Kauvar,[‡] Gordon Wetzstein,[‡] and Mark L. Brongersma[*,†]

[†]Geballe Laboratory for Advanced Materials, Stanford University, Stanford, California 94305-4045, United States
[‡]Department of Electrical Engineering, Stanford University, Stanford, California 94305, United States

S Supporting Information

ABSTRACT: Three-dimensional (3D) single-particle tracking (SPT) is a key tool for studying dynamic processes in the life sciences. However, conventional optical elements utilizing light fields impose an inherent trade-off between lateral and axial resolution, preventing SPT with high spatiotemporal resolution across an extended volume. We overcome the typical loss in spatial resolution that accompanies light-field-based approaches to obtain 3D information by placing a standard microscope coverslip patterned with a multifunctional, light-field metasurface on a specimen. This approach enables an otherwise unmodified microscope to gather 3D information at an enhanced spatial resolution. We demonstrate simultaneous tracking of multiple fluorescent particles within a large $0.5 \times 0.5 \times 0.3$ mm^3 volume using a standard epi-fluorescent microscope with submicron lateral and micron-level axial resolution.

KEYWORDS: Light-field metasurface, interleaved metasurface, single-particle tracking, Mie resonance, microlens array, point spread function engineering
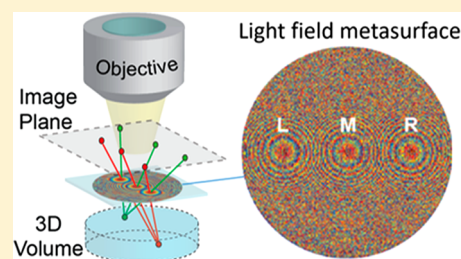
Single particle tracking (SPT) is a powerful technique with applications across disciplines including biology and fluid dynamics. Protein movement, gene trafficking, cellular interactions, drug delivery, and turbulent fluid flow can be probed using SPT approaches, with the advantage that local, individual dynamics can be recovered, rather than ensemble averages.[1−9] Many approaches to achieve three-dimensional SPT rely upon the use of microlens arrays (MLAs) in light-field imaging to simultaneously record both lateral and axial information about the location of individual fluorescent particles.[10] The numerical aperture (NA) of the lenses in the MLA is quite limited, as they cannot physically overlap. This results in an inherent trade-off between the lateral and axial spatial resolutions. Several methods have aimed to overcome this drawback. Deconvolution algorithms that incorporate pixel-count super-resolution have been developed to reconstruct 3D volumes with improved spatial resolution, but these approaches struggle to maintain resolution uniformity across their depth and suffer from a diffraction-induced resolution limit.[11−13] Wavefront coding techniques[14−16] utilizing point spread function (PSF) engineering enable high axial resolution but have a limited depth of field or a lateral resolution limited by the MLA used for generating the light field. A different approach for simultaneous 3D imaging is based on bi-[17−20] or multiplane microscopy using diffractive optical elements,[21] but this methodology only provides high-resolution image information on a limited number of discrete planes and does not capture the angular information on a full 4D light field that can be beneficial for localization or specimen characterization.

To make further progress, it is critical to develop novel optical components that are not constrained by the very limited design space of conventional optics.

Metasurfaces consist of dense arrangements of resonant optical antennas and offer tremendous freedom in manipulating optical wave-fronts by imparting subwavelength, space-variant phase-changes on incident electromagnetic waves.[22−35] Recently, a number of groups have reported the experimental realization of dielectric metasurface optical elements capable of delivering high transmission efficiencies in the visible spectrum.[25,33,34,36−42] More recently, it was demonstrated how interleaved metasurface optical elements can achieve multiple functions within the same shared aperture.[43−48] In addition to being ultrathin and compact, these multifunctional metasurfaces can provide entirely new functions that are impossible to achieve with conventional optical components— hence, they are fitting candidates to break the assumed dichotomy between high lateral and axial resolution in volumetric imaging.

Results and Discussion. In this work, we propose the concept of a light-field metasurface (LM) to track the 3D location of fluorescent emitters in an aqueous volume (Figure 1a) with high spatial resolution and in real time. We construct the LM by randomly interleaving three metalenses on the basis
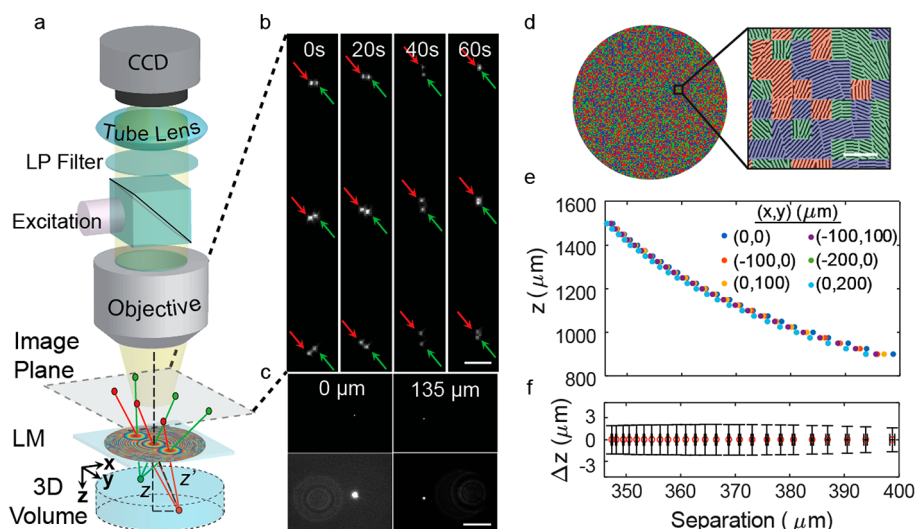
Figure 1. (a) Schematic layout of the LM imaging two beads at different (x, y, z) locations. (b) Images corresponding to two fluorescent beads formed by the LM captured at 20 s intervals. Arrows of the same color indicate subimages corresponding to the same bead. The scale bar is 35 μm. (c) Images of the two fluorescent beads without the LM separated by a height of 135 μm. In each image, one of the beads is moved into focus (top). Images with an adjusted brightness and contrast to facilitate observation of the darker, out-of focus bead (bottom). The scale bar is 8 μm. (d) Schematic of the LM (left) comprised of three metasurface lenses that are spatially interleaved within a single 200 μm-diameter aperture. A false-colored SEM (right) showing the distinct hyperbolic phase profiles (red, green, and blue) of three lenses that are offset by 66 μm and then discretized into 600 nm squares. The scale bar is 1 μm. (e) Measured separations between the top and bottom images from a single bead at various (x, y) locations in the 3D volume in μm. (f) Depth uncertainties in the z-direction at each location derived from uncertainties of the Gaussian fits of a single fluorescent bead centered LM central optical axis, where $(x, y) = (0, 0)$.

of the geometric or Pancharatnam–Berry phase within a 200 μm-diameter shared aperture. Their optical axes are linearly spaced with a separation of 66 μm (Figure 1a,d) (see Supporting Information section S1). The axes offsets lead to the formation of three spatially separated, replicated images at the image plane of the LM. These images are readily captured by a charge-coupled device (CCD) attached to a conventional optical microscope with a 50× 0.8 NA objective. When two closely spaced 1 μm-diameter fluorescent beads (λ = 532 nm) are optically excited with a 480 nm pump, the LM produces six separated fluorescence images of the beads (Figure 1b) that can be tracked as they diffuse in the liquid. By removing the LM from the microscope and finding the plane of best-focus for each observed bead, we determined that these beads were separated in the z-direction by approximately 135 μm (Figure 1c). Without the benefits of interleaving, due to the extreme separation between these two beads, it is impossible to directly determine their 3D positions in a single measurement. Due to the optical axis offsets of each lens, three different perspectives are achieved in a single image. The depth information on each bead is directly translated to lateral information in the subimages (see Supporting Information section S2). Therefore, we can obtain depth information for each particle by measuring the lateral separation between the two outermost bead images. Figure 1e shows how this separation changes when a stationary bead is scanned in the z-direction by a stepper stage. By using the trajectory scanned along the z-axis (where (x, y) is $(0, 0)$), we can calibrate the LM to determine a look-up table between the radial (z') and depth (z) distances (Figure 1a and Supporting Information eq S5). With this table, the lateral (x, y) location of the bead can be calculated with the help of a simple particle localization algorithm based on linear coordinate scaling at each radial depth (see Supporting Information section S3). Hence, by measuring the central

image location and outer bead image separation, we obtain the full 3D (x, y, z) position information.

Using algorithms developed for localization-based super-resolution microscopy, we can determine the localization uncertainty of each imaged bead.[49] The lateral uncertainty of each bead is given by[50]

$$\langle (\Delta x)^2 \rangle = \frac{\sigma^2 + a^2/12}{N} + \frac{8\pi\sigma^4 b^2}{a^2 N^2} \tag{1}$$

where σ is the fitted standard deviation of the intensity profile, a is the image-projected pixel size, b is the background signal level, and N is the number of photon counts. The first part of this expression accounts for photon-counting and pixelated noise, while the latter captures the impact of background noise of the CCD. We cascade the uncertainty in the lateral dimensions through the particle localization algorithm to give the axial uncertainty for each particle image. Figure 1e shows the uncertainty in the z values for a bead scanned along the center optical axis, showing axial uncertainties less than 2.5 μm over the entire 600 μm depth of field.

One of the primary advantages of using an interleaved LM is the enhancement in spatial resolution afforded by maintaining a large numerical aperture for each sublens. This enables one to effectively localize and separate fluorescent particles by reducing the likelihood of aliasing among the images of fluorescent markers. A conventional MLA is constrained to allow only a single phase profile within a given aperture, but in an interleaved LM, all three metalenses can share the entire aperture and thereby capture higher in-plane wave vector components. This comes at the expense of a decreased intensity proportional to $1/N^2$, where N is the number of interleaved lenses.[51] For a MLA, light is equally shared among each lens, leading to an achievable intensity scaling proportional to $1/N$. In order to mitigate the impact of a reduced intensity due to the interleaving, we choose to only use three
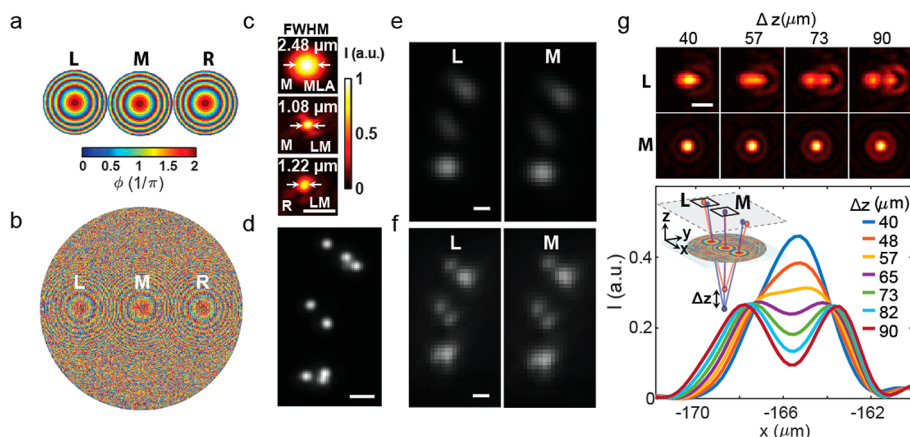
Figure 2. (a, b) Phase profiles of a non-interleaved (a) MLA and (b) LM three lenses with optical axes separated by 66 μm. (c) Experimentally measured focal spots from plane wave illumination in the (x, y) plane for the middle (M) and right (R) lens corresponding to the MLA (upper) and LM (center and lower) with the FWHM labeled. The illumination wavelength was 600 nm, and the scale bar is 3 μm. (d) A cluster of 1 μm beads imaged by a commercial 100× objective with a NA of 0.9. The scale bar is 4 μm. (e, f) Images of the beads shown in panel d formed with the L and M lenses from the (e) MLA and (f) LM lenses. The scale bar is 4 μm. (g) Simulated images from the L and M lenses of the LM from two beads with a center of mass of 760 μm from the LM (top) with the beads separated by Δz and centered along the optical axis (inset). Intensity profiles from lens L for increasing values of Δz (lower plot).
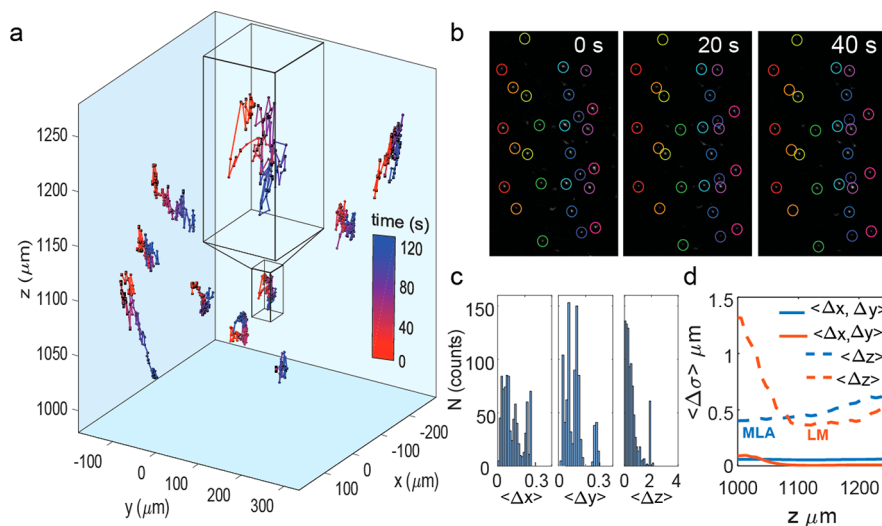

Figure 3. (a) Experimental trajectories of nine fluorescent beads simultaneously tracked in real time. The black error bars indicate the location uncertainty based on the Gaussian fitting of the peak locations. The inset is a $50 \times 50 \times 140$ μm³ window showing a single bead trajectory. (b) Images formed by the LM at selected times used to construct the (x, y, z) locations for each particle. (c) Histograms of the cumulative uncertainties for each spatial coordinate for all tracked particles. (d) Simulated uncertainties for the experimental conditions shown in panel a comparing the MLA and LM performance.

lenses in our proof-of-concept and compare the performance to a non-overlapping MLA with lens diameters equal to the separation of the optical axis of the LM. A more favorable scaling in intensity may soon be achievable, as many groups are pursuing higher-performance interleaving approaches.[45] Parts a and b of Figure 2 show the phase profiles of a non-interleaved MLA and a LM. In this case, the lateral diffraction-limited resolution of the LM can theoretically be 3 times higher than the MLA due to the increased numerical aperture achieved through multiplexing.

In order to characterize the resolution difference between the MLA and LM lenses, we first measured the full width at half-maximum (FWHM) of the focal spots in the (x, y) plane upon plane wave illumination and found the FWHM to be improved from 2.48 to 1.08 μm by multiplexing three lenses into one (Figure 2c). The benefits of a reduced FWHM are

clearly demonstrated when a cluster of fluorescent beads are imaged under the same viewing conditions (Figure 2d−f). We employ Fourier optics (see Supporting Information section S2) to simulate the case of two close, laterally spaced point sources and find that the minimum resolvable bead separation is reduced from 2.1 to 0.8 μm by interleaving the lenses with the scheme illustrated in Figure 2a,b. The spatial resolution of the LM can be further improved as the numerical aperture of the lenses is increased in the LM design, but at the cost of a reduction in the achievable depth of field. In this work, we chose a numerical aperture of 0.44 for the sublenses in the LM, allowing us to resolve beads that are more than 800 nm apart while maintaining a substantial 250 μm depth of field. The axial resolution of the LM along the z-axis determines the minimum resolvable separation between two beads along the same radial line of sight. Figure 2g shows the simulated images

of a pair of beads centered along the optical axis and located 760 μm from the LM with varying z separations (Figure 2g). As the separation between the two beads gets larger, due to the axial offset of side lenses, the L and R images begin to form two bead images. We are able to distinguish two beads when the side L and R images meet the Rayleigh criterion. This occurs at z separations greater than 73 μm for any bead distance spanning 600−900 μm from the LM (Supporting Information Figure S4). The vast majority of the time, beads will also have lateral offsets that will allow them to be located with ±2.5 μm accuracy across the 250 μm depth of field (Figure 1f).

We pattern an LM directly on a coverslip and place it on top of a droplet of water containing a dilute concentration of fluorescent beads, enabling us to simultaneously track the 3D location of all of the beads in our field of view. Figure 3a shows the trajectory of nine particles tracked over the course of 2 min within a $0.5 \times 0.5 \times 0.3$ mm^3 volume (see Supporting Information Videos S1 and S2). The three images obtained from each individual bead are grouped and labeled by three similarly colored circles, as illustrated in Figure 3b. The localization uncertainties are determined at each time for every tracked particle using eq 1 using Gaussian fitting of the imaged beads (Figure 3c). The lateral uncertainties are less than 300 nm, while the axial uncertainties are less than 2 μm, which is similar to the calculated uncertainties for this LM, which outperforms the MLA in both lateral and axial uncertainties for a majority of the depth of field (Figure 3d) (see Supporting Information section S5). These location uncertainties could be slightly reduced to the uncertainties predicted by Fourier optics if the subresolution particles were used (∼750 nm particles for this LM).

A peak-fitting-based approach to determine each particle's location uncertainty is useful for simultaneous tracking of particles, but this approach does not provide the lower bound on the absolute best uncertainty performance of the lens. In order to deduce the lowest possible location uncertainty, we use the Fisher information from a single particle imaged at all axial locations by the MLA and LM lenses. This method takes into account the information gathered over an entire image volume captured by the lens. We calculate the Cramér−Rao bound (CRB) which is the inverse of the Fisher information, and it expresses the lower bound on the variance of the location of a point source imaged by the lens.[52] The square root of this bound gives the maximum particle location uncertainty similar to the uncertainty shown in eq 1 except it is based on the information available in the entire image. The CRB predicts that the MLA and LM have similar lateral and axial uncertainties, but the MLA has a greater depth of field (Supporting Information Figure S6). For the case of tracking multiple independent particles, the CRB is not a useful measure of the lens performance because it gives the location uncertainty for a single point source. When a localized fitting method is used, the higher NA and moderate intensities produced by the LM yield better localization performance for each particle.

In conclusion, we demonstrate that, by interleaving multiple optical elements into a light-field metasurface, we can circumvent the inherent trade-off between spatial and depth resolution in conventional light-field imaging to enable high-resolution 3D particle tracking within an extended volume. We further demonstrate that synchronous 3D imaging can be achieved without substantially modifying the optical system of a conventional optical microscope simply by adding a patterned coverslip to the top of a fluorescent sample specimen.

■ ASSOCIATED CONTENT

Ⓢ Supporting Information

The Supporting Information is available free of charge on the ACS Publications website at DOI: 10.1021/acs.nanolett.8b04673.

> Supplementary Video S1 showing fluorescent beads diffusing through an aqueous channel viewed at the image plane of the IML with a 20× microscope objective (NA = 0.4) (the colored circles indicate individual beads that have been identified in each frame; each frame is 1 s in duration) (AVI)

> Supplementary Video S2 showing three-dimensional trajectories of nine fluorescent beads shown in Supplementary Video S1 (AVI)

> Supplementary text, Table S1, and Figures S1−S6 related to the design principle for a high NA light-field metasurface, imaging using a conventional lenslet array, the coordinate transformation algorithm, Fourier imaging simulations, and comparison of the localization uncertainty for MLA and LM lenses (PDF)

■ AUTHOR INFORMATION

Corresponding Author
*E-mail: brongersma@stanford.edu.

ORCID Ⓞ
Dianmin Lin: 0000-0001-8343-9120
Mark L. Brongersma: 0000-0003-1777-8970

Author Contributions
§A.L.H. and D.L. contributed equally to this work. A.L.H., D.L., and M.L.B. conceived the concept of the paper. D.L designed the metasurface lens. A.L.H. fabricated the lens and conducted the optical measurements. A.L.H. and I.K. performed Fourier imaging simulations and wrote the particle-tracking algorithm. All authors worked on the manuscript. M.L.B supervised the project.

Notes
The authors declare no competing financial interest.

■ REFERENCES

(1) Maas, H. G.; Gruen, A.; Papantoniou, D. *Exp. Fluids* **1993**, *15*, 133−146.
(2) Saxton, M. J.; Jacobson, K. *Annu. Rev. Biophys. Biomol. Struct.* **1997**, *26*, 373−399.
(3) Adrian, R. J. *Exp. Fluids* **2005**, *39*, 159−169.
(4) Saxton, M. J. *Nat. Methods* **2008**, *5*, 671−672.
(5) Dehmelt, L.; Bastiaens, P. I. H. *Nat. Rev. Mol. Cell Biol.* **2010**, *11*, 440.
(6) Suh, J.; Dawson, M.; Hanes, J. *Adv. Drug Delivery Rev.* **2005**, *57*, 63−78.

(7) Manzo, C.; Garcia-Parajo, M. F. *Rep. Prog. Phys.* **2015**, *78*, 124601.

(8) Sergé, A.; Bertaux, N.; Rigneault, H.; Marguet, D. *Nat. Methods* **2008**, *5*, 687.

(9) Jaqaman, K.; Loerke, D.; Mettlen, M.; Kuwata, H.; Grinstein, S.; Schmid, S. L.; Danuser, G. *Nat. Methods* **2008**, *5*, 695−702.

(10) Pégard, N. C.; Liu, H.-Y.; Antipa, N.; Gerlock, M.; Adesnik, H.; Waller, L. *Optica* **2016**, *3*, 517.

(11) Broxton, M.; Grosenick, L.; Yang, S.; Cohen, N.; Andalman, A.; Deisseroth, K.; Levoy, M. *Opt. Express* **2013**, *21*, 25418−25439.

(12) Prevedel, R.; Yoon, Y.-G.; Hoffmann, M.; Pak, N.; Wetzstein, G.; Kato, S.; Schrödel, T.; Raskar, R.; Zimmer, M.; Boyden, E. S.; Vaziri, A. *Nat. Methods* **2014**, *11*, 727−730.

(13) Kauvar, I.; Chang, J.; Wetzstein, G. In *IEEE ICCP*; IEEE, 2017; pp 1−12.

(14) Cohen, N.; Yang, S.; Andalman, A.; Broxton, M.; Grosenick, L.; Deisseroth, K.; Horowitz, M.; Levoy, M. *Opt. Express* **2014**, *22*, 24817−24839.

(15) Shechtman, Y.; Sahl, S. J.; Backer, A. S.; Moerner, W. E. *Phys. Rev. Lett.* **2014**, *113*, 133902.

(16) Shechtman, Y.; Weiss, L. E.; Backer, A. S.; Lee, M. Y.; Moerner, W. E. *Nat. Photonics* **2016**, *10*, 590−594.

(17) Toprak, E.; Balci, H.; Blehm, B. H.; Selvin, P. R. *Nano Lett.* **2007**, *7*, 2043−2045.

(18) Prabhat, P.; Ram, S.; Ward, E. S.; Ober, R. J. *IEEE Trans. Nanobioscience* **2004**, *3*, 237−242.

(19) Badieirostami, M.; Lew, M. D.; Thompson, M. A.; Moerner, W. E. *Appl. Phys. Lett.* **2010**, *97*, 161103.

(20) Hou, S.; Lang, X.; Welsher, K. *Opt. Lett.* **2017**, *42*, 2390−2393.

(21) Abrahamsson, S.; Chen, J.; Hajj, B.; Stallinga, S.; Katsov, A. Y.; Wisniewski, J.; Mizuguchi, G.; Soule, P.; Mueller, F.; Darzacq, C. D.; Darzacq, X.; Wu, C.; Bargmann, C. I.; Agard, D. A.; Dahan, M.; Gustafsson, M. G. L. *Nat. Methods* **2013**, *10*, 60−63.

(22) Verslegers, L.; Catrysse, P. B.; Yu, Z. F.; White, J. S.; Barnard, E. S.; Brongersma, M. L.; Fan, S. H. *Nano Lett.* **2009**, *9*, 235−238.

(23) Yu, N. F.; Genevet, P.; Kats, M. A.; Aieta, F.; Tetienne, J. P.; Capasso, F.; Gaburro, Z. *Science* **2011**, *334*, 333−337.

(24) Arbabi, A.; Horie, Y.; Bagheri, M.; Faraon, A. *Nat. Nanotechnol.* **2015**, *10*, 937−943.

(25) Lin, D. M.; Fan, P. Y.; Hasman, E.; Brongersma, M. L. *Science* **2014**, *345*, 298−302.

(26) Lalanne, P.; Astilean, S.; Chavel, P.; Cambril, E.; Launois, H. *Opt. Lett.* **1998**, *23*, 1081−1083.

(27) Lalanne, P.; Astilean, S.; Chavel, P.; Cambril, E.; Launois, H. *J. Opt. Soc. Am. A* **1999**, *16*, 1143−1156.

(28) Pors, A.; Albrektsen, O.; Radko, I. P.; Bozhevolnyi, S. I. *Sci. Rep.* **2013**, *3*, 2155.

(29) Shalaev, M. I.; Sun, J.; Tsukernik, A.; Pandey, A.; Nikolskiy, K.; Litchinitser, N. M. *Nano Lett.* **2015**, *15*, 6261−6266.

(30) Fattal, D.; Li, J. J.; Peng, Z.; Fiorentino, M.; Beausoleil, R. G. *Nat. Photonics* **2010**, *4*, 466−470.

(31) Hasman, E.; Kleiner, V.; Biener, G.; Niv, A. *Appl. Phys. Lett.* **2003**, *82*, 328−330.

(32) Arbabi, A.; Horie, Y.; Ball, A. J.; Bagheri, M.; Faraon, A. *Nat. Commun.* **2015**, *6*, 7069.

(33) Ni, X.; Kildishev, A. V.; Shalaev, V. M. *Nat. Commun.* **2013**, *4*, 2807.

(34) Chen, X. Z.; Huang, L. L.; Muhlenbernd, H.; Li, G. X.; Bai, B. F.; Tan, Q. F.; Jin, G. F.; Qiu, C. W.; Zhang, S.; Zentgraf, T. *Nat. Commun.* **2012**, *3*, 198.

(35) Yin, X. B.; Ye, Z. L.; Rho, J.; Wang, Y.; Zhang, X. *Science* **2013**, *339*, 1405−1407.

(36) Khorasaninejad, M.; Chen, W. T.; Devlin, R. C.; Oh, J.; Zhu, A. Y.; Capasso, F. *Science* **2016**, *352*, 1190−1194.

(37) Devlin, R. C.; Khorasaninejad, M.; Chen, W. T.; Oh, J.; Capasso, F. *Proc. Natl. Acad. Sci. U. S. A.* **2016**, *113*, 10473−10478.

(38) Zhan, A.; Colburn, S.; Trivedi, R.; Fryett, T. K.; Dodson, C. M.; Majumdar, A. *ACS Photonics* **2016**, *3*, 209−214.

(39) Lalanne, P.; Chavel, P. *Laser Photonics Rev.* **2017**, *11*, 1600295.

(40) Yu, Y. F.; Zhu, A. Y.; Paniagua-Domínguez, R.; Fu, Y. H.; Luk'yanchuk, B.; Kuznetsov, A. I. *Laser Photon. Rev.* **2015**, *9*, 412−418.

(41) Deng, Z.-L.; Zhang, S.; Wang, G. P. *Opt. Express* **2016**, *24*, 23118.

(42) Astilean, S.; Lalanne, P.; Chavel, P.; Cambril, E.; Launois, H. *Opt. Lett.* **1998**, *23*, 552.

(43) Lin, D.; Holsteen, A. L.; Maguid, E.; Wetzstein, G.; Kik, P. G.; Hasman, E.; Brongersma, M. L. *Nano Lett.* **2016**, *16*, 7671−7676.

(44) Veksler, D.; Maguid, E.; Shitrit, N.; Ozeri, D.; Kleiner, V.; Hasman, E. *ACS Photonics* **2015**, *2*, 661−667.

(45) Maguid, E.; Yulevich, I.; Veksler, D.; Kleiner, V.; Brongersma, M. L.; Hasman, E. *Science* **2016**, *352*, 1202.

(46) Maguid, E.; Yulevich, I.; Yannai, M.; Kleiner, V.; L Brongersma, M.; Hasman, E. *Light: Sci. Appl.* **2017**, *6*, No. e17027.

(47) Arbabi, E.; Arbabi, A.; Kamali, S. M.; Horie, Y.; Faraon, A. *Optica* **2016**, *3*, 628−633.

(48) Khorasaninejad, M.; Capasso, F. *Nano Lett.* **2015**, *15*, 6709−6715.

(49) Deschout, H.; Cella Zanacchi, F.; Mlodzianoski, M.; Diaspro, A.; Bewersdorf, J.; Hess, S. T.; Braeckmans, K. *Nat. Methods* **2014**, *11*, 253−266.

(50) Thompson, R. E.; Larson, D. R.; Webb, W. W. *Biophys. J.* **2002**, *82*, 2775−2783.

(51) Maguid, E.; Yulevich, I.; Veksler, D.; Kleiner, V.; Brongersma, M. L.; Hasman, E. *Science* **2016**, *352*, 1202−1206.

(52) Lew, M. D.; Thompson, M. A.; Badieirostami, M.; Moerner, W. E. *Proc. SPIE-Int. Soc. Opt. Eng.* **2010**, *7571*, No. 75710Z.